ACS APPLIED MATERIALS & INTERFACES

Research Article

www.acsami.org

Synthetic Control of Composition and Crystallite Size of Silver Hollandite, $Ag_xMn_8O_{16}$: Impact on Electrochemistry

Kenneth J. Takeuchi,*[,†] Shali Z. Yau,[‡] Melissa C. Menard,[§] Amy C. Marschilok,*[,†,§] and Esther S. Takeuchi*[,†,§]

[†]Department of Chemistry and [§]Department of Materials Science and Engineering, Stony Brook University (SUNY), Stony Brook, New York 11794, United States

[‡]Department of Chemistry, University at Buffalo (SUNY), Buffalo, New York 14260, United States

Stony Brook University (SUNY), Stony Brook, New York 11794, United States

Supporting Information

ABSTRACT: Synthetic control of the silver content in silver hollandite, $Ag_xMn_8O_{16}$, where the silver content ranges from $1.0 \leq x \leq 1.8$ is demonstrated. This level of compositional control was enabled by the development of a lower temperature reflux based synthesis compared to the more commonly reported hydrothermal approach. Notably, the synthetic variance of the silver content was accompanied by a concomitant variance in crystallite size as well as surface area and particle size. To verify the retention of the hollandite structure, the first Rietveld analysis of silver hollandite was conducted on samples of varying composition. The impacts of silver content, crystallite size, surface area, and particle size on electrochemical reversibility were examined under cyclic voltammetry and battery testing.

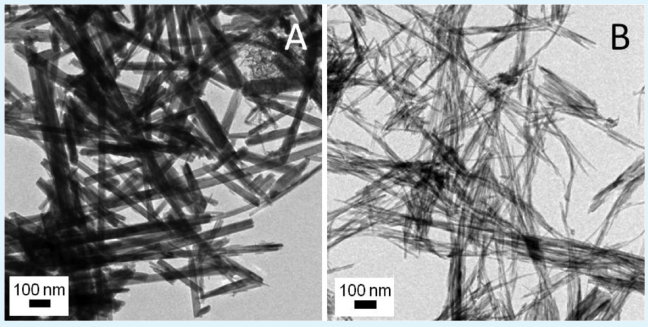

KEYWORDS: *silver hollandite, crystallite size control, reflux synthesis, compositional control, Rietveld analysis, electrochemistry, battery*

INTRODUCTION

Hollandite (cryptomelane) structured minerals are an important geological structure type in the Earth's lower crust and upper mantle.[1,2] Hollandite type materials consist of octahedral units of edge-sharing manganese oxide octahedra (MnO_6) which interlink to form tunnels of 2 × 2 (0.46 nm) dimensions.[3] The Mn cations within the structure possess mixed 3+ and 4+ oxidation states. Bimetallic materials have been prepared that contain cations that are 1+ or 2+ and partially occupy locations within the manganese oxide tunnels to stabilize charge.[4,5] Usually, cations of alkali metals and alkaline earth metals, such as K^+, Rb^+, and Ba^{2+} occupy the centers of the tunnels,[6] but hollandite-type manganese oxides containing other interstitial metal ions such as Cr^{3+} have also been reported.[7]

Hollandites are an intriguing class of manganese oxides as the tunnel structure provides a robust framework for insertion and deinsertion of ions and small molecules, allowing them to function as sorbents and catalysts under a wide array of applications.[8−13] Similarly, secondary batteries such as lithium-ion systems are dependent on facile Li^+ movement in the electroactive cathode. Thus conceptually, hollandite structured materials would provide an appropriate framework for utilization as secondary (rechargeable) battery materials.[14] Silver hollandite is particularly appealing in this regard, as the Ag^+ center has the potential to be electrochemically active.

Despite the natural abundance of hollandite structured materials, the preparation of pure silver hollandite has remained elusive. The synthesis of silver hollandite was first described in 1984 via a high temperature, high pressure solid-state route.[15,16] The product was a mixture of $Ag_{1.8}Mn_8O_{16}$, Mn_2O_3, and Ag_2O. The next reported synthesis appeared in 2005, where silver hollandite was prepared by applying a post ion exchange treatment to crypto- melane (KMn_8O_{16}) in the presence of excess silver nitrate ($AgNO_3$).[10] While silver hollandite was generated at lower temperatures using this approach, potassium (K) residue was detected in the product, at significant (1.5−7.3 molar %) levels. Metallic silver (Ag^0) was also detected by X-ray diffraction and transmission electron microscopy, which the authors attributed to decomposition of excess $AgNO_3$ during the high-temperature calcination step. Even after refining the synthesis, the authors concluded that silver hollandite free of trace Ag metal impurity could not be prepared using an ion-exchange approach. An additional solid state synthesis was reported in 2008,[17] where a low temperature solid state reaction of $AgMnO_4$ and manganese(II) acetate tetrahydrate ($Mn(C_2H_3O_2)_2{\cdot}4H_2O$) produced silver hollandite. The silver hollandite made by this method was less crystalline than the

Received: July 24, 2012
Accepted: September 27, 2012
Published: October 9, 2012

   dx.doi.org/10.1021/am301443g | ACS Appl. Mater. Interfaces 2012, 4, 5547−5554

potassium analog prepared using a comparable solid state approach.[18] Calcination of the silver hollandite material at 300 °C had little effect on the crystallinity, while calcination at 800 °C resulted in formation of distinct Ag and Mn_2O_3 phases.[17]

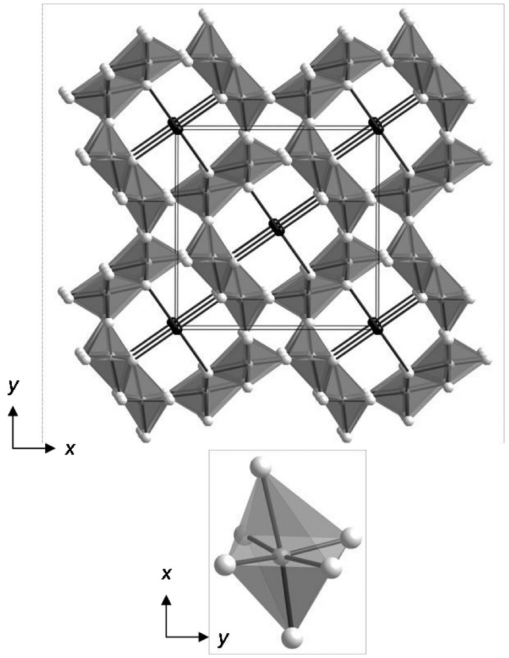

Figure 1. Silver hollandite structure, $Ag_{1.56}Mn_8O_{16}$, depicted with Ag atoms as black spheres that occupy the center of the channels created by edge-sharing MnO_6 octahedra.

Hydrothermal syntheses of silver hollandite were reported in 2007[19] and in 2011,[20] utilizing silver permanganate ($AgMnO_4$) and manganese nitrate ($Mn(NO_3)_2$) as reagents. Contrary to the ion exchange method discussed above, no diffraction peaks due to metallic Ag^0 were detected for silver hollandite prepared using the hydrothermal method. A reflux based synthesis for preparation of silver hollandite was described in 2007,[21] which incorporated a high temperature calcination step. Although the major phase produced was silver hollandite, significant pyrolusite (β-MnO_2) impurity was evident in the product.

We recently reported a novel reflux preparation and the first electrochemical assessment of silver hollandite.[22] The information provided here illustrates our ability to tune the material properties of silver hollandite ($Ag_xMn_8O_{16}$) via modifications in the reflux synthesis conditions. To verify that our conditions generate structurally consistent silver hollandite, the first Rietveld analysis of silver hollandite is also reported herein. Notably, we emphasize in this report that hydrothermal reaction conditions, the typical synthetic conditions for the production of hollandite materials, do not allow for a complete variance in Ag to Mn ratios, while maintaining the hollandite structure.

With a change in Ag to Mn ratios, we also observe a concomitant variance in crystallite size and associated particle size and bulk surface area. This ability to synthetically control material properties enabled the systematic exploration of the fundamental properties of silver hollandite, which reveals a dependence of electrochemical reversibility on chemical or physical properties, likely crystallite size. In a more general sense, fundamental studies involving the impact of physical and chemical properties of materials on their electrochemical properties are critical in the rational development of materials, which may address the present and future requirements for stationary and portable power.

EXPERIMENTAL SECTION

Silver hollandite was prepared using two different synthetic methods, hydrothermal and ambient pressure reflux reactions. Reagents used in the synthesis were silver permanganate ($AgMnO_4$), nitric acid (HNO_3), and manganese sulfate monohydrate ($MnSO_4{\cdot}H_2O$) whose ratios were varied, as discussed below. The as prepared samples were washed with DI water and dried in vacuo.[22]

Characterization of silver hollandite samples was conducted utilizing several methods including inductively coupled plasma spectrometry-optical emission spectroscopy (ICP-OES), scanning electron microscopy (SEM), energy dispersive X-ray spectroscopy (EDS), transmission electron microscopy (TEM), simultaneous thermogravimetric analysis/differential scanning calorimetry (TGA/DSC), X-ray powder diffraction (XRD), surface area by gas adsorption (BET) and particle size by light scattering. MDI JADE version 8.5.3 software was used with ICDD and NIST databases for search-match analysis.

X-ray diffraction (XRD) data were collected at room temperature with a Rigaku Ultima-IV system (Cu Kα radiation) with Bragg–Brentano configuration. X-ray diffraction patterns of all samples were indexed to $Ag_{1.8}Mn_8O_{16}$.[23] Crystallite sizes of silver hollandite samples were estimated by applying the Scherrer equation[24,25] to the (211) peak of the XRD data, after correcting for instrumental broadening using a LaB_6 standard.

Rietveld structure refinement of selected samples was performed using the software package GSAS and the EXPGUI interface.[26,27] The profile was fit using Thompson-Cox-Hastings pseudo-Voigt profile function and the background was fit using a shifted Chebyshev polynomial with 6 terms.[28,29] Atomic positions from single crystal refinement of the previously reported silver hollandite ($Ag_{1.8}Mn_8O_{16}$) were used as starting positions.[15,16] The occupancy of Ag was initially set to values consistent with the Ag concentration determined from inductively coupled plasma-optical emission spectroscopy. The atomic displacement parameters were refined isotropically (U_{iso}) with the U_{iso} of the O atoms constrained to be equivalent. The anisotropic crystallite sizes, or average crystal dimensions, both along the length of the Mn–O tunnel and across the width of the Mn–O tunnel were calculated from the (2 1 1) and (1 3 0), respectively, using the Scherrer equation.[30,31]

A Hitachi S-800 model was used for SEM and EDS data collection with secondary electron images acquired at 20 and 25 kV. Brunauer–Emmett–Teller surface area (BET) data was collected using N_2(g) as adsorbent. Particle size data was collected using laser light scattering methodology. Transmission electron microscopy (TEM) was collected in a JEOL JEM 2010 with an accelerating voltage of 200 kV, and a point resolution of 0.19 nm.

For electrochemical testing, the electrolyte used was a mixture of propylene carbonate and dimethoxyethane containing 1 M lithium hexafluoroarsenate ($LiAsF_6$). Cyclic voltammetry data were collected at room temperature utilizing a three electrode configuration with lithium reference and auxiliary electrodes. A scan rate of 1.00×10^{-4} V/s was used with voltage limits of 3.7 and 2.0 V. Three consecutive voltammetric scans were collected. Two electrode test cells were fabricated using lithium as the negative electrode and the galvanostatic intermittent titration type (GITT) tests were conducted at 30 °C, where the $Ag_xMn_8O_{16}$ material was electrochemically reduced via intermittent application of a 0.0063 mA/cm^2 load for 2 h followed by a period of open circuit rest.

RESULTS AND DISCUSSION

Material Synthesis. We have investigated the hydrothermal approach for the preparation of silver hollandite and note here the preparation of pure silver hollandite ($Ag_xMn_8O_{16}$) where the silver content ranges from $1.3 \leq x \leq 1.5$. Attempts to prepare silver hollandite with lower silver

content via hydrothermal methods resulted in pyrolusite (β-MnO_2) as the predominant product (Figure 2). Pyrolusite (β-MnO_2) is the most thermodynamically stable form of MnO_2,[1,32] and has been observed previously as a byproduct in prior hydrothermal syntheses of silver hollandite.[19] We recently introduced a novel reflux based method for the synthesis of pure silver hollandite, achieving a nanocrystalline material at low temperatures without calcination.[22] The first systematic investigation of the reflux synthesis of silver hollandite is described here. Notably, via reflux we were able to form pure silver hollandite ($Ag_xMn_8O_{16}$) where the silver content (x) could be varied from $1.0 \leq x \leq 1.8$ (Figures 3, 4).

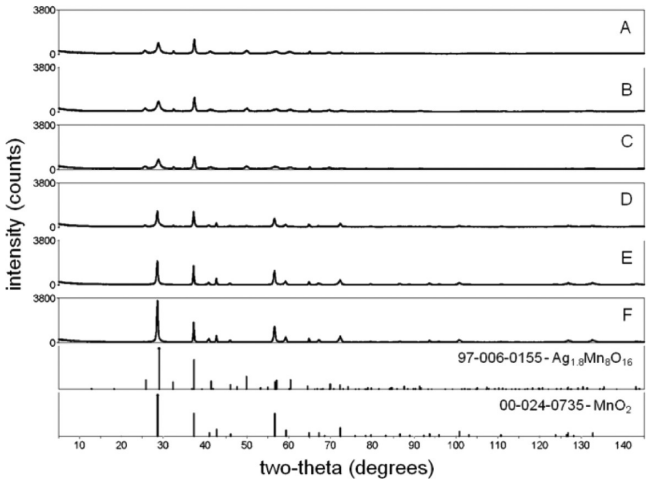

Figure 2. X-ray diffraction for samples prepared via hydrothermal reaction with x in $Ag_xMn_8O_{16}$ = (a) 1.50, (b) 1.48, (c) 1.33; and β-MnO_2 with Ag/8Mn = (d) 0.49, (e) 0.02, and (f) 0.01.

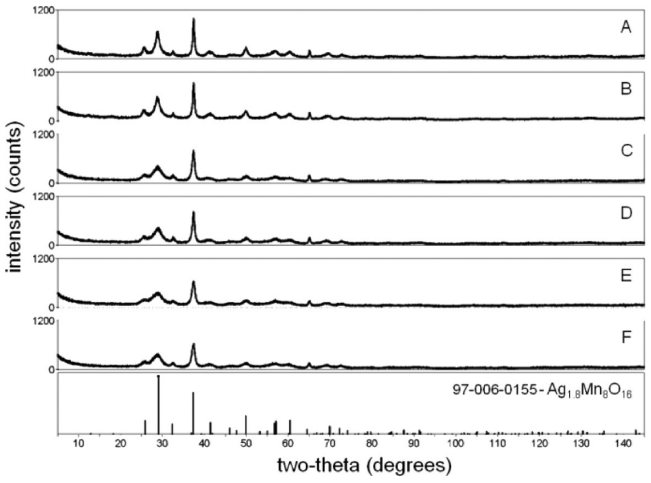

Figure 3. X-ray diffraction for samples prepared via reflux reaction with x in $Ag_xMn_8O_{16}$ = (a) 1.64, (b) 1.56, (c) 1.53, (d) 1.45, (e) 1.31, and (f) 1.13.

We postulate that the reflux method enables a broader compositional range because it makes formation of the thermodynamically favored β-MnO_2 less likely than under higher temperature hydrothermal conditions.

The stoichiometry of our material samples was determined by inductively coupled plasma-optical emission spectroscopy (ICP-OES). No residual K^+ was detected by ICP-OES analysis

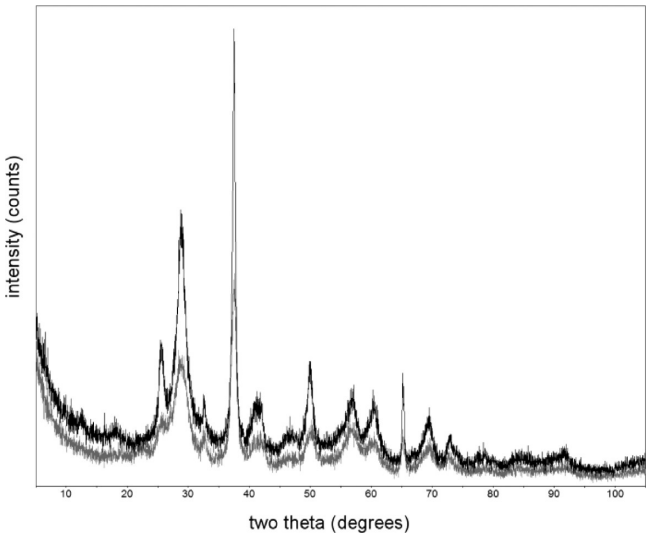

Figure 4. X-ray diffraction for samples prepared via reflux reaction with x in $Ag_xMn_8O_{16}$ = 1.08 (gray) and 1.79 (black).

for any of our synthetic products. Notably, we have established that the reflux approach shows clear advantages over the hydrothermal method in terms of synthetic versatility, where a broader compositional range of silver content (x) in the desired silver hollandite ($Ag_xMn_8O_{16}$) product could be achieved (Figure 5). Thus, reflux was selected as the preparation method

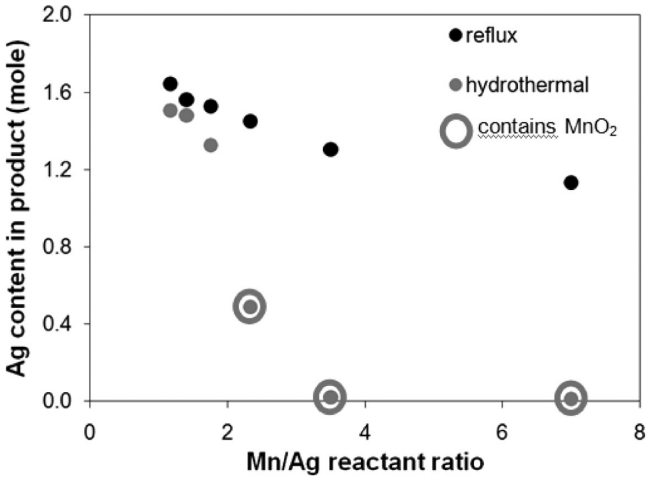

Figure 5. Comparison of reflux and hydrothermal syntheses of silver hollandite ($Ag_xMn_8O_{16}$).

of choice for the other material characterization, structure analysis, and electrochemical evaluation studies described here.

Material Characterization. A correlation was observed between the silver content (x) and the crystallite size of the silver hollandite ($Ag_xMn_8O_{16}$) material as determined by X-ray diffraction (XRD) (Figure 6). Lower silver content samples ($Ag_{1.0}Mn_8O_{16}$) had crystallite sizes of ~10−11 nm while the samples with the higher silver content ($Ag_{1.8}Mn_8O_{16}$) had crystallite sizes of ~20−25 nm. Samples with intermediate silver content showed intermediate crystallite size. This trend was observed for over 140 samples that were synthesized where the most significant increase in crystallite size was observed for samples where $x > 1.5$ in $Ag_xMn_8O_{16}$.

dx.doi.org/10.1021/am301443g | ACS Appl. Mater. Interfaces 2012, 4, 5547−5554

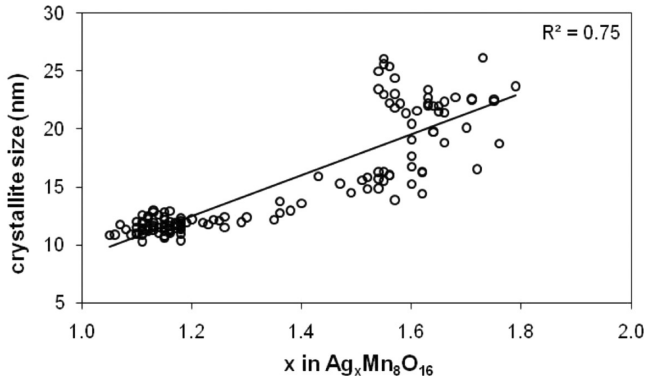

Figure 6. Crystallite size of silver hollandite ($Ag_xMn_8O_{16}$) as a function of silver content (x).

Notably, the control of the silver content (x) in the silver hollandite ($Ag_xMn_8O_{16}$) material also led to modification of physical parameters as well.

Surface areas were determined by gas adsorption using the BET method. There was a general trend of decreasing surface area with increasing silver content and crystallite size (Figure 7). For example, samples with silver content of x = 1.73 in

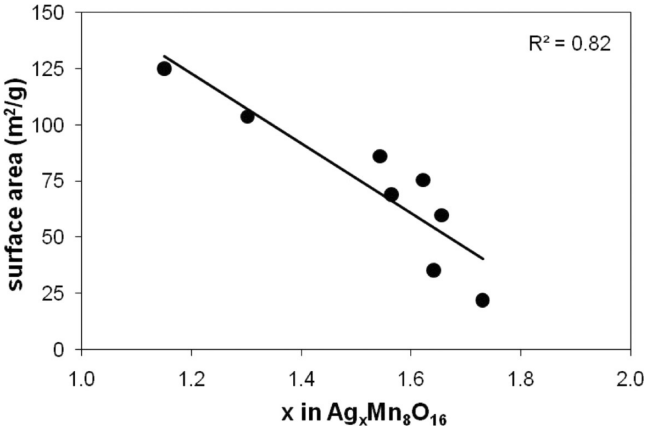

Figure 7. Surface area of silver hollandite ($Ag_xMn_8O_{16}$) as a function of silver content (x).

$Ag_xMn_8O_{16}$ and a crystallite size of 26.1 nm showed surface areas of 22 m^2/g, whereas the samples with silver content of x = 1.15 in $Ag_xMn_8O_{16}$ and a crystallite size of 10.5 nm showed a surface area of 125 m^2/g. Particle sizes of the samples were measured using light scattering. Interestingly, a trend of increasing particle size with decreasing silver content and crystallite size was observed (Figure 8). Small crystallites have a greater surface area to volume ratio than large crystallites, and therefore possess less inherent stability than large sized crystallites. Thus, smaller crystallites would be expected to have a greater tendency to aggregate, and form precipitates of larger particle size when suspended in a liquid. This relationship of small crystallite size material yielding larger particle size has been previously observed with magnetite, Fe_3O_4.[33] Thermogravimetric analysis was used to determine the water content of the silver hollandite samples. The water content per formula unit was determined by the mass loss up to 360 °C, a temperature where water should fully desorb but no structural decomposition should occur, based on prior thermogravimetric analysis–mass spectrometry studies.[19] The average water

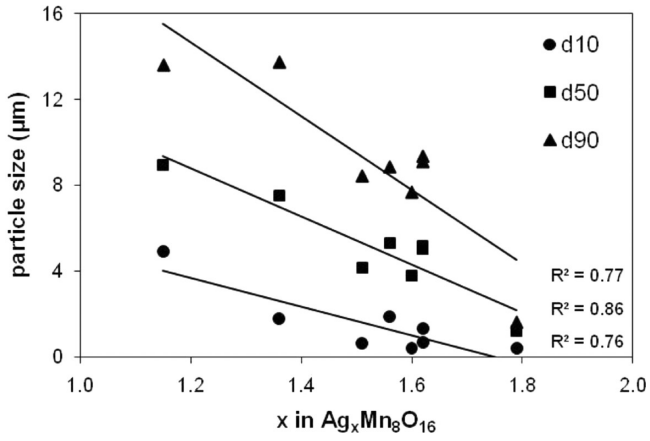

Figure 8. Particle size of silver hollandite ($Ag_xMn_8O_{16}$) as a function of silver content (x).

content per formula unit for 45 samples was 1.87 H_2O with a standard deviation of 0.31. There was no trend noted with water content related to the silver content in the formula.

The crystallization mechanism of potassium cryptomelane (hollandite) has been studied by TEM, where longitudinal and lateral growth of the particles were proposed to proceed by different mechanisms.[34] Temperature and pH were found to be controlling parameters in the prior work. To investigate the effect of silver composition, TEM images of silver hollandite samples with the compositions of $Ag_{1.46}Mn_8O_{16}$ and $Ag_{1.10}Mn_8O_{16}$ were recorded under magnifications of 10 000×. Both material samples displayed high length to width aspect ratios with a highly acicular appearance. The resulting representative images illustrate a clear difference between typical samples with high and low silver content (Figure 9). The higher silver content $Ag_{1.46}Mn_8O_{16}$ sample displayed long nanorods with some short nanorods present that ranged from 100 nm to 1 μm long and about 20 nm wide. The lower silver content $Ag_{1.10}Mn_8O_{16}$ sample features appeared more like fibers or whiskers because of their small diameter. This material also displayed long nanorods with a somewhat higher population of short nanorods that were 10 nm wide and 100 nm to 1 μm long.

Overall, control of the silver content in the $Ag_xMn_8O_{16}$ ($1.0 \leq x \leq 1.8$) was accompanied by accompanying changes of crystallite size, surface area, particle size and the diameter of the acicular particles. Thus, control of both the material composition and physical properties was enabled by the reflux based synthetic approach.

Structure Analysis. In 1984, a single crystal structure of $Ag_{1.8}Mn_8O_{16}$ was reported, where the material was prepared using a high temperature method.[15,16] Silver hollandite can be described as a 1D tunnel consisting of double chains of edge-sharing MnO_6 octahedra. The cube-like cavities are created by face-sharing cubes of O^{2-} atoms with Ag atoms occupying the shared faces of the O^{2-} cubes. The occupancy of the Ag atoms at the shared faces of the cube-like cavities yields a peculiar square planar Ag^+ environment with bond distances of approximately 2.7 Å, which are a little larger than Ag^+–O^{2-} (2.35 Å).[35]

We report for the first time the Rietveld refinement of silver hollandite (Figure 10, Tables 1–3). The small crystallite size, low crystallinity, and anisotropic nature of the crystalline morphology in our $Ag_{1.56}Mn_8O_{16}$ and $Ag_{1.15}Mn_8O_{16}$ materials

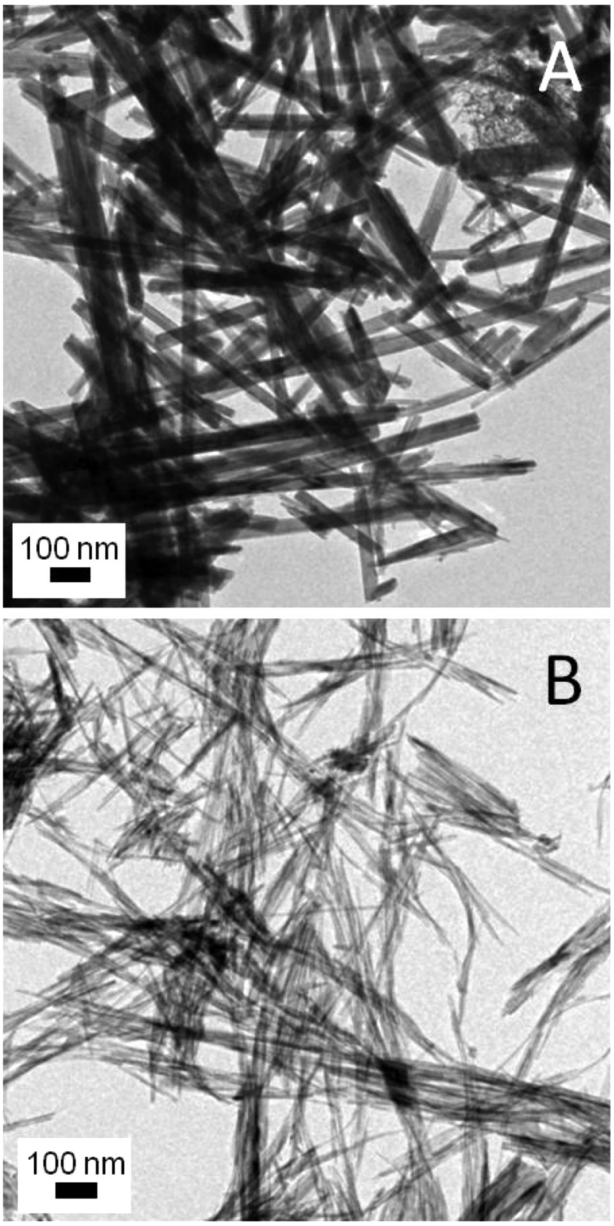

Figure 9. Transmission electron microscope images of silver hollandite ($Ag_xMn_8O_{16}$), 10 000× magnification for x = (A) 1.46, (B) 1.10.

resulted in broad diffraction peaks with pronounced anisotropic strain perpendicular to the c-axis. Broadening of this nature in the powder X-ray diffraction peaks of nanosized materials is not unexpected. These results are consistent with previous reports of Rietveld refinement of structurally similar, nanosized materials such as $Fe_{7.6}Ni_{0.4}O_{6.35}(OH)_{9.65}Cl_{1.25}$,[36] $K_2(M,Sn)_8O_{16}$,[37] $LiFeO_2$,[38] α-MnO_2,[39] and KMn_8O_{16}.[40]

Because the previously reported single-crystal data describes high silver content silver hollandite ($Ag_{1.8}Mn_8O_{16}$),[15,16] we selected two lower silver content samples for Rietveld refinement ($Ag_{1.56}Mn_8O_{16}$ and $Ag_{1.15}Mn_8O_{16}$), in order to assess any structural differences in the lower silver content materials. The MnO_6 octahedra are similar yet more distorted in our $Ag_{1.56}Mn_8O_{16}$ and $Ag_{1.15}Mn_8O_{16}$ materials compared with the previous report for $Ag_{1.8}Mn_8O_{16}$, where the smaller bond distances and angles coincide with the shared-edge common to two octahedra on each side of the tunnel.[23]

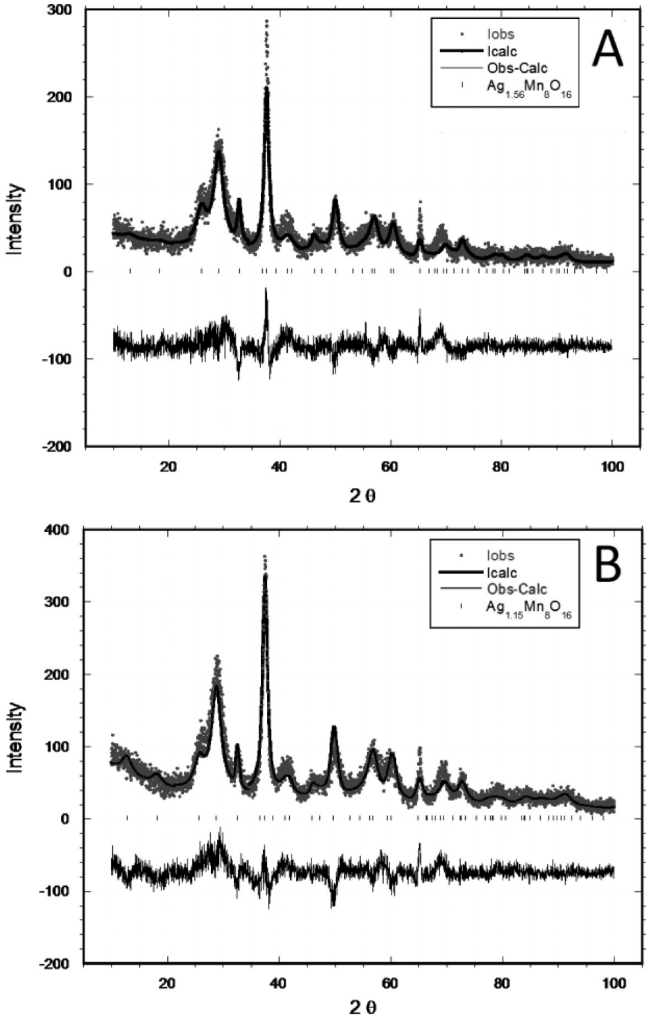

Figure 10. Rietveld refinement results for silver hollandite ($Ag_xMn_8O_{16}$) samples at 10 000× magnification with x = (A) 1.56, (B) 1.15.

Table 1. Crystallographic Data and Rietveld Refinement Results for Silver Hollandite ($Ag_xMn_8O_{16}$)

chemform	$Ag_{1.56}Mn_8O_{16}$	$Ag_{1.15}Mn_8O_{16}$
cryst syst	tetragonal	tetragonal
space group	$I4/m$	$I4/m$
Z	1	1
a (Å)	9.756(10)	9.831(11)
c (Å)	2.858(6)	2.872(6)
V (Å^3)	272.0(8)	277.6(8)
R_{wp}[a]	0.2097	0.1821
R_p[a]	0.1647	0.1439
χ^2	1.688	1.878
S[a]	1.30	1.39
2θ range (deg)	10−100	10−100
2θ step width (deg	0.020	0.025
no. of reflns	85	85
water content (mol)	2.4	2.4
crystallite size (211) (nm)	18.4(1)	11.7(1)
crystallite size (130) (nm)	3(1)	3(1)

[a]The R factors and S are defined in ref 41.

Model calculations have shown that a hollandite crystal can contain a large variety of arrangements of octahedral cations in

dx.doi.org/10.1021/am301443g | ACS Appl. Mater. Interfaces 2012, 4, 5547−5554

Table 2. Atomic Positions in Silver Hollandite ($Ag_xMn_8O_{16}$)

atom	site	x	y	z	U_{iso} (Å^2)[a]	Occ.[b]
			$Ag_{1.56}Mn_8O_{16}$			
Ag	2a	0	0	0	0.0273	0.78
Mn	8h	0.1493	0.3321	0.5	0.0068	1.0
O1	8h	0.1599	0.2075	0	0.0095	1.0
O2	8h	0.1311	0.4708	0	0.0094	1.0
			$Ag_{1.15}Mn_8O_{16}$			
Ag	2a	0	0	0	0.0273	0.58
Mn	8h	0.1493	0.3321	0.5	0.0068	1.0
O1	8h	0.1517	0.1953	0	0.0095	1.0
O2	8h	0.1356	0.4620	0	0.0094	1.0

[a] U_{iso} is the isotropic atomic displacement parameter when the Debye–Waller factor is represented as $\exp(-8\pi^2 U \sin^2\theta/\lambda^2)$. [b] Occupancy.

Table 3. Selected Interatomic Distances (Å) in Silver Hollandite ($Ag_xMn_8O_{16}$)

Mn–O1(×1)	Ag–O1(×4)	Mn–O2(×2)	Mn–O1(×2)	Mn–O2(×1)
		$Ag_{1.56}Mn_8O_{16}$		
1.901(4)	1.976(3)	1.879(3)	1.778(4)	2.555(5)
		$Ag_{1.15}Mn_8O_{16}$		
1.975(4)	1.927(3)	1.968(3)	1.869(4)	2.431(5)

different unit cells and a corresponding range of tunnel-cation positions.[11] It has been noted that if different unit cells within the hollandite crystal contain a variety of arrangements of octahedral cations, a corresponding range of tunnel-cation positions will arise, causing the positional disorder observed for the tunnel-cation sites in X-ray structure refinements. Comparison of the XRD patterns of our $Ag_{1.56}Mn_8O_{16}$ and $Ag_{1.15}Mn_8O_{16}$ materials to the previously reported $Ag_{1.8}Mn_8O_{16}$ material indicates a systematic broadening of some diffraction peaks in our materials. Interestingly, significant broadening is observed in crystallographic planes which bisect the tunnels and intersect silver atoms ((220), (130), (101), (440), and (600)), with significantly less broadening for diffraction peaks which do not intersect silver atoms ((211), (411), and (611)). Because the silver atoms are positioned in the tunnel locations, it is intuitive that the crystallographic planes which intersect silver atoms would exhibit greater broadening than the planes which do not intersect silver atoms. For example, the (130) plane is representative of all the planesthat cut through the length of the tunnel and in-tersect the row of central Ag atoms, and the (211)plane is representative of all the planes that cut through the width of the tunnel and do not intersect the row of central Ag atoms (Figure 11).

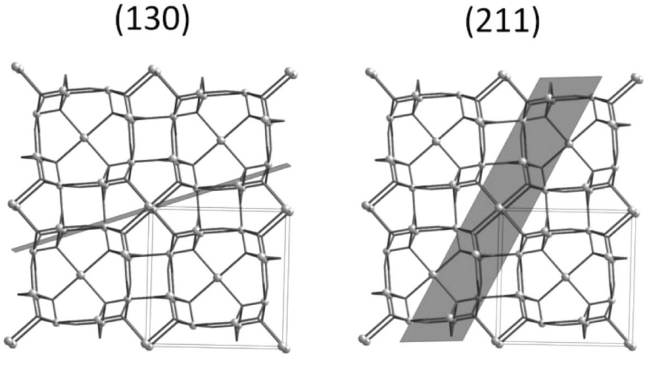

Figure 11. (130) and (211) for silver hollandite ($Ag_xMn_8O_{16}$).

Electrochemical Evaluation. The electrochemical properties of silver hollandite had not been previously studied prior to our initial report evaluating possible application of silver hollandite as a battery cathode material.[22] Our discharge/charge cycling tests showed a first cycle discharge capacity of 180 mA h/g, and encouraging preliminary cycling results, with reasonable capacity retention after an initial larger first cycle capacity loss. An additional electrochemical investigation of silver hollandite was described in 2011, where a first discharge capacity of 166 mA h/g, and a cycle 30 discharge capacity of 100 mA h/g were observed,[20] all consistent with our prior report.

For this study, silver hollandite samples representative of low and high crystallite sizes and silver contents were selected, for the first evaluation of material effects on electrochemical properties of $Ag_xMn_8O_{16}$. As discussed above, modification of the silver content resulted in concomitant effects on the crystallite size, particle size, and surface area of the materials. The materials are discussed in the context of crystallite size in this section of the manuscript. However, it is noted that the other material properties may also have an important impact on the resulting electrochemistry.

Cyclic voltammetry data were collected for two samples of $Ag_xMn_8O_{16}$ where x = 1.55 and 1.23 with corresponding crystallite sizes of 25.6 and 12.1 nm, respectively (Figure 12). Three consecutive cycles of data were collected. For both the small crystallite size material and the large crystallite size material, one anodic peak and one cathodic peak were observed on each cycle. In both cases, the peak current for the cathodic peak in the first cycle was larger than the cathodic peak in the second cycle (Table 5). The peak currents for the cathodic and anodic peaks for the second scan and the third scan were more consistent indicating that Ag-hollandite material is able to successfully undergo multiple reduction–oxidation processes.

More detailed examination of the voltammograms for the materials of large and small crystallite size reveals notable differences. The smaller crystallite size $Ag_{1.23}Mn_8O_{16}$ sample displayed more closely spaced anodic and cathodic peak voltages than the larger crystallite size $Ag_{1.55}Mn_8O_{16}$ sample, illustrating a higher level of electrochemical reversibility for small crystallite size materials Additionally, the peak current per gram for the small crystallite size material was higher than that for the large crystallite size material (Figure 12) indicating an improved ability to deliver higher current for the smaller crystallite size material.

Silver hollandite samples of compositions $Ag_{1.55}Mn_8O_{16}$ and $Ag_{1.25}Mn_8O_{16}$ with crystallite sizes of 25.6 and 12.1 nm, respectively, were used to construct two electrode cells using lithium metal as the anode. The cells were tested in a Galvanostatic Intermittent Titration (GITT) type scheme. The cells assembled using the smaller crystallite sized $Ag_{1.25}Mn_8O_{16}$ material consistently displayed loaded voltages several hundred millivolts higher than the cells with the larger crystallite $Ag_{1.55}Mn_8O_{16}$ material (Figure 13). As a consequence, the cells with the smaller crystallite size material delivered 354 mAh/g to 2.0 V compared to the larger crystallite size sample that delivered 186 mA h/g. These results affirm the observation of improved electrochemical behavior from the voltammetry data that smaller crystallite size silver hollandite provides higher delivered ampere hours per gram. In this case, tuning the material during the synthesis process enabled the cells to deliver almost twice (1.9×) the ampere hours per gram.

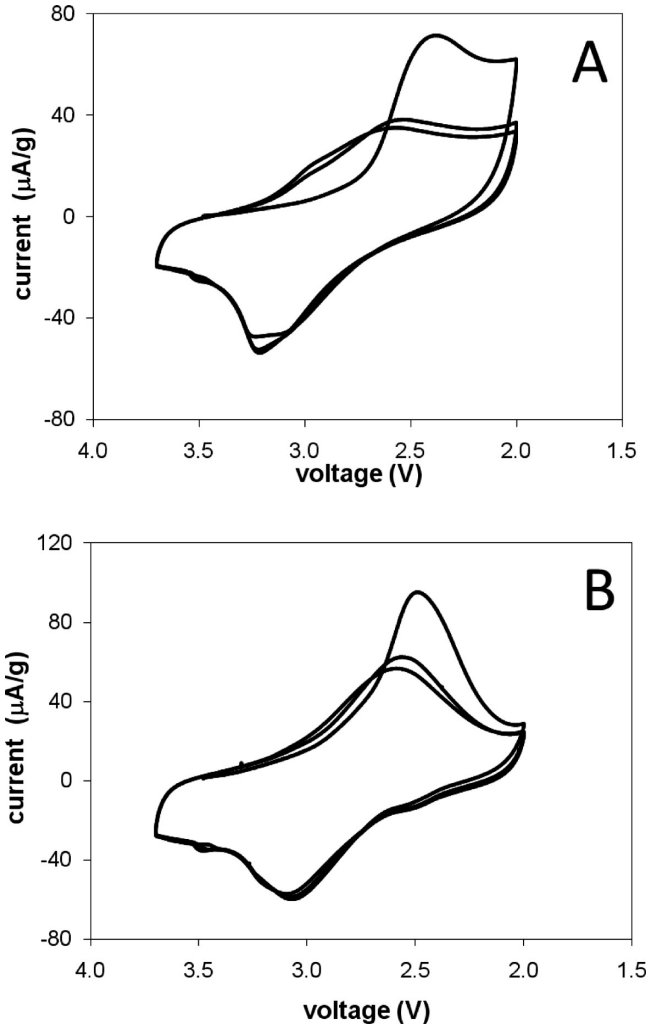

Figure 12. Cyclic voltammetry for silver hollandite ($Ag_xMn_8O_{16}$), with x = (A) 1.55 and (B) 1.23 versus lithium.

Table 5. Cathodic (E_{pc}) and Anodic (E_{pa}) Peak Voltages by Cycle Number for Silver Hollandite ($Ag_xMn_8O_{16}$)

	E_{pc} (V)			E_{pa} (V)		
x	1	2	3	1	2	3
1.23	2.49	2.57	2.58	3.07	3.07	3.10
1.55	2.37	2.54	2.58	3.24	3.22	3.21

SUMMARY

In summary, a lower temperature, scalable, reflux-based synthesis of pure silver hollandite has been successfully demonstrated, where the structure purity of the various silver hollandite products is verified via the first Rietveld analysis of silver hollandite. The silver content and related physical properties were tunable by varying the reactant Ag:Mn ratio where the Ag content (x) in silver hollandite ($Ag_xMn_8O_{16}$) could be varied from $1.0 \leq x \leq 1.8$, with retention of overall structure.

The modification of the material by reducing crystallite size and increasing surface area showed profound effects on the resultant electrochemistry with increased reversibility for the low silver content, small crystallite size samples and an almost doubling of delivered ampere hours per gram. This work affirms our conceptual strategy that physical and chemical variations of materials can have profound impacts on electrochemical properties critical to the rational design of material chemistries appropriate for power storage systems.

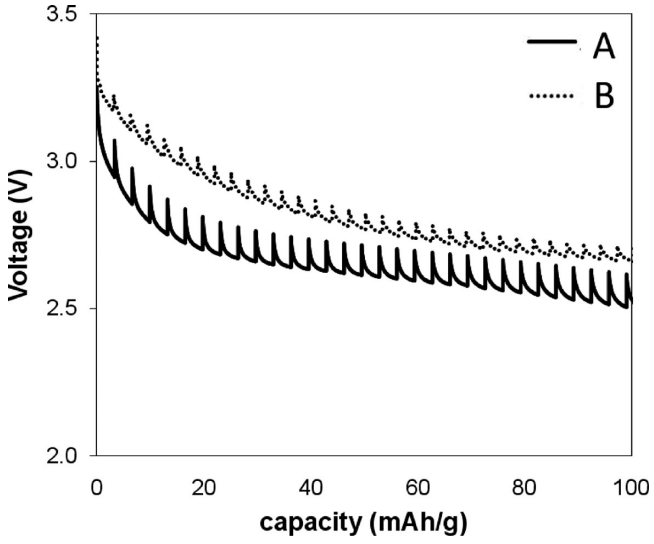

Figure 13. Galvanostatic intermittent titration (GITT) type test, initial discharge for lithium/silver hollandite ($Ag_xMn_8O_{16}$) electrochemical test cells, with x = (A) 1.55 and (B) 1.25.

ASSOCIATED CONTENT

Supporting Information

Structural data used in the Rietveld analysis is available as a crystallographic information file (CIF). This material is available free of charge via the Internet at http://pubs.acs.org.

AUTHOR INFORMATION

Corresponding Author

*E-mail: kenneth.takeuchi.1@stonybrook.edu (K.J.T.); amy.marschilok@stonybrook.edu (A.C.M.); esther.takeuchi@stonybrook.edu (E.S.T.).

Author Contributions

The manuscript was written through contributions of all authors. All authors have given approval to the final version of the manuscript.

Notes

The authors declare no competing financial interest.

ACKNOWLEDGMENTS

This work was supported by the Department of Energy, Office of Basic Energy Sciences, under Grant DE-SC0002460. Galvanostatic intermittent titration-type (GITT) testing for possible use as a primary cell was supported by National Institutes of Health under Grant 1R01HL093044-01A1 from the National Heart, Lung, and Blood Institute. Rietveld analysis of the manganese compounds was funded by the New York State Energy Research and Development Authority, NYSERDA, agreement 18517. The authors thank Corey P. Schaffer for assistance with cyclic voltammetry measurements.

REFERENCES

(1) Post, J. E. *Proc. Natl. Acad. Sci. U.S.A.* **1999**, *96*, 3447−3454.
(2) Gruner, J. W. *Am. Mineral.* **1943**, *28* (9−10), 497−506.
(3) Ching, S.; Suib, S. L. *Comm. Inorg. Chem.* **1997**, *19* (5), 263−282.
(4) Vicat, J.; Fanchon, E.; Strobel, P.; Duc Tran, Q. *Acta Crystallogr., Sect. B* **1986**, *B42*, 162−167.

(5) Ozawa, T.; Suzuki, I.; Sato, H. *J. Phys. Soc. Jpn.* **2006**, *75* (1), 014802−1−014802−8.
(6) Brock, S. L.; Duan, N.; Tian, Z. R.; Giraldo, O.; Zhou, H.; Suib, S. L. *Chem. Mater.* **1998**, *10* (10), 2619−2628.
(7) Ching, S.; Driscoll, P. F.; Kieltyka, K. S.; Marvel, M. R.; Suib, S. L. *Chem. Commun.* **2001**, *23*, 2486−2487.
(8) Nicolas-Tolentino, E.; Tian, Z.-R.; Zhou, H.; Xia, G.; Suib, S. L. *Chem. Mater.* **1999**, *11* (7), 1733−1741.
(9) Tsuji, M.; Komarneni, S. *J. Mater. Res.* **1993**, *8* (3), 611−616.
(10) Li, L.; King, D. L. *Chem. Mater.* **2005**, *17* (17), 4335−4343.
(11) Dyer, A.; Pillinger, M.; Newton, J.; Harjula, R.; Möller, T.; Amin, S. *Chem. Mater.* **2000**, *12* (12), 3798−3804.
(12) Dharmarathna, S.; King'ondu, C. K.; Pedrick, W.; Pahalagedara, L.; Suib, S. L. *Chem. Mater.* **2012**, *24* (4), 705−712.
(13) Huang, H.; Sithambaram, S.; Chen, C.-H.; King'ondu Kithongo, C.; Xu, L.; Iyer, A.; Garces, H. F.; Suib, S. L. *Chem. Mater.* **2010**, *22* (12), 3664−3669.
(14) Feng, Q.; Kanoh, H.; Miyai, Y.; Ooi, K. *Chem. Mater.* **1995**, *7* (1), 148−153.
(15) Chang, F. M.; Jansen, M. *Angew. Chem., Int. Ed.* **1984**, *23* (11), 906−907.
(16) Chang, F. M.; Jansen, M. *Rev. Chim. Miner.* **1986**, *23* (1), 48−54.
(17) Chen, J.; Li, J.; Li, H.; Huang, X.; Shen, W. *Microporous Mesoporous Mater.* **2008**, *116* (1−3), 586−592.
(18) Ding, Y.-s.; Shen, X.-F.; Sithambaram, S.; Gomez, S.; Kumar, R.; Crisostomo, V. M. B.; Suib, S. L.; Aindow, M. *Chem. Mater.* **2005**, *17*, 5382−5389.
(19) Sandhu, S. S.; Brutchen, G. W.; Fellner, J. P. *J. Power Sources* **2007**, *170* (1), 196−209.
(20) Sun, Y.; Hu, X.; Zhang, W.; Yuan, L.; Huang, Y. *J. Nanopart. Res.* **2011**, *13*, 3139−3148.
(21) Chen, J.; Li, J.; Liu, Q.; Huang, X.; Shen, W. *Chin. J. Catal.* **2007**, *28* (12), 1034−1036.
(22) Zhu, S.; Marschilok, A. C.; Lee, C.-Y.; Takeuchi, E. S.; Takeuchi, K. J. *Electrochem. Solid-State Lett.* **2010**, *13* (8), A98−A100.
(23) Chang, F. M.; Jansen, M. *Angew. Chem., Int. Ed.* **1984**, *23*, 906−907.
(24) Scherrer, P. *Nachr. Ges. Wiss. Gottingen* **1918**, 96−100.
(25) Patterson, A. L. *Phys. Rev.* **1939**, *56*, 978−82.
(26) Larson, A. C.; Von Dreele, R. B. *General Structure Analysis System (GSAS)*; Los Alamos National Laboratory Report LAUR 86-748 ; Los Alamos National Laboratory: Los Alamos, NM, 2000.
(27) Toby, B. H. *J. Appl. Crystallogr.* **2001**, *34*, 210−213.
(28) Howard, C. J. *J. Appl. Crystallogr.* **1982**, *15*, 615−620.
(29) Thompson, P.; Cox, D. E.; Hastings, J. B. *J. Appl. Crystallogr.* **1987**, *20*, 79−83.
(30) Scherrer, P. *Göttinger Nachr. Ges.* **1918**, *2*, 98.
(31) Patterson, A. L. *Phys. Rev.* **1939**, *56* (10), 978−982.
(32) Greedan, J. E.; Raju, N. P.; Wills, A. S.; Morin, C.; Shaw, S. M.; Reimers, J. N. *Chem. Mater.* **1998**, *10* (10), 3058−3067.
(33) Zhu, S.; Marschilok, A. C.; Takeuchi, E. S.; Takeuchi, K. J. *Electrochem. Solid-State Lett.* **2009**, *12* (4), A91−A94.
(34) Portehault, D.; Cassaignon, S.; Baudrin, E.; Jolivet, J.-P. *Chem. Mater.* **2007**, *19* (22), 5410−5417.
(35) Shannon, R. D. *Acta Crystallogr., Sect. A* **1976**, *32*, 751−768.
(36) Post, J. E.; Buchwald, V. F. *Am. Mineral.* **1991**, *76*, 272−277.
(37) Sharma, N.; Plévert, J.; Subba Rao, G. V.; Chowdari, B. V. R.; White, T. J. *Chem. Mater.* **2005**, *17* (18), 4700−4710.
(38) Matsumura, T.; Kanno, R.; Inaba, Y.; Kawamoto, Y.; Takano, M. *J. Electrochem. Soc.* **2002**, *149* (12), A1509−A1513.
(39) Kijima, N.; Takahashi, Y.; Akimoto, J.; Awaka, J. *J. Solid State Chem.* **2005**, *178* (9), 2741−2750.
(40) Xiao, T. D.; Bokhimi; Benaissa, M.; Pérez, R.; Strutt, P. R.; Yacamán, M. J. *Acta Mater.* **1997**, *45* (4), 1685−1693.
(41) Young, R. A. *The Rietveld Method*; Oxford University Press: Oxford, U.K., 1995.